THE JOURNAL OF BIOLOGICAL CHEMISTRY VOL. 288, NO. 35, pp. 25551–25561, August 30, 2013

Structural Basis of a Physical Blockage Mechanism for the Interaction of Response Regulator PmrA with Connector Protein PmrD from *Klebsiella pneumoniae*[*]

Received for publication, May 1, 2013, and in revised form, July 13, 2013 Published, JBC Papers in Press, July 16, 2013, DOI 10.1074/jbc.M113.481978

Shih-Chi Luo[‡], Yuan-Chao Lou[‡], Mahalingam Rajasekaran[‡], Yi-Wei Chang[§], Chwan-Deng Hsiao[§], and Chinpan Chen[‡¶1]

From the Institutes of [‡]Biomedical Sciences and [§]Molecular Biology, Academia Sinica, Taipei 115, Taiwan and [¶]Agricultural Biotechnology Center, National Chung Hsing University, Taichung 40227, Taiwan

Background: PmrD binds to phospho-PmrA and sustains its phosphorylation state.
Results: Phospho-PmrA interacts with PmrD via several specific intermolecular interactions.
Conclusion: A steric inhibition mechanism was proposed for protecting phospho-PmrA against dephosphorylation.
Significance: This work provides novel data revealing how a connector protein protects an activated response regulator.

In bacteria, the two-component system is the most prevalent for sensing and transducing environmental signals into the cell. The PmrA-PmrB two-component system, responsible for sensing external stimuli of high Fe^{3+} and mild acidic conditions, can control the genes involved in lipopolysaccharide modification and polymyxin resistance in pathogens. In *Klebsiella pneumoniae*, the small basic connector protein PmrD protects phospho-PmrA and prolongs the expression of PmrA-activated genes. We previously determined the phospho-PmrA recognition mode of PmrD. However, how PmrA interacts with PmrD and prevents its dephosphorylation remains unknown. To address this question, we solved the x-ray crystal structure of the N-terminal receiver domain of BeF_3^--activated PmrA ($PmrA_N$) at 1.70 Å. With this structure, we applied the data-driven docking method based on NMR chemical shift perturbation to generate the complex model of PmrD-$PmrA_N$, which was further validated by site-directed spin labeling experiments. In the complex model, PmrD may act as a blockade to prevent phosphatase from contacting with the phosphorylation site on PmrA.

For all organisms, sensing and responding to environmental cues is essential to their survival. Compared with eukaryotic signaling cascades, which are mainly involved in mediating signals through specific Ser-, Thr-, and Tyr-phosphorylated residues among the related sub-tracts, in prokaryotic signaling systems, a distinct phosphorylation scheme predominates, the two-component system (TCS)[2] (1–3). Hundreds of TCSs have been found in eubacteria, archaea, and a few eukaryotic organisms (4), and the TCS is the most prevalent system in bacteria for transducing external information into the cell and coping with environmental stresses (2, 5). A PmrA-PmrB TCS, dealing with cationic antimicrobial peptides and polymyxin resistance in pathogens (6), is responsible for sensing the external stimuli caused directly or indirectly by excess Fe^{3+}, low Mg^{2+}, and mild acidic environments (7–9). Under this TCS, pathogens can alter the composition of their cell walls to resist neutralization of polymyxin for drug resistance and allow bacterial survival within macrophages by reducing the affinity with cationic antimicrobial peptides (10, 11).

The increasing antibiotic resistance to *Klebsiella pneumonia* bacteria, a common cause of nosocomial bacterial infections causing pneumonia and urinary tract infections, especially in immunocompromised patients (12), led us to investigate how the virulence and drug resistance persist via the associated TCS. Similar to most response regulators, the PmrA of *K. pneumoniae* belonging to the OmpR-PhoB family is composed of an N-terminal receiver domain (Fig. 1) and a C-terminal effector/DNA-binding domain. Interestingly, at low Mg^{2+} concentration, the PhoP-PhoQ system promotes the expression of a small basic protein, PmrD (7), which can prevent the intrinsic dephosphorylation of phospho-PmrA and enhance the expression of PmrA-activated downstream genes (13). Therefore, PmrD is termed a "connector" because it connects the PmrA-PmrB and PhoP-PhoQ systems (14). Besides PmrD, other small-sized proteins that connect TCSs for *Escherichia coli* include SafA, which connects the PhoP-PhoQ and EvgS-EvgA systems (15); IraM, which connects PhoP-PhoQ and binds to response regulator RssB, thereby preventing the proteins from recruiting targets for degradation (16); and MzrA, which connects CpxR-Cpxa and OmpR-EnvZ systems (17). To date, the complicated mechanisms of cross-regulation among these TCSs are still not clear (14), and no detailed structural information is available about how the phosphorylation site of the

* This work was supported by grants from Academia Sinica and the National Science Council (NSC 97-2311-B-001-013-MY3) in Taiwan and in part by the Ministry of Education (Taiwan) under the ATU plan.

The atomic coordinates and structure factors (code 3W9S) have been deposited in the Protein Data Bank (http://wwpdb.org/).

Chemical shifts of $PmrA_N$ were deposited in the BioMagResBank under accession number BMRB 18922.

[1] To whom correspondence should be addressed: Institute of Biomedical Sciences, Academia Sinica, 128 Academia Rd., Section 2, Taipei 115, Taiwan. Tel.: 886-2-2652-3035; Fax: 886-2-2788-7641; E-mail: bmchinp@ibms.sinica.edu.tw.

[2] The abbreviations used are: TCS, two-component system; PmrA, polymyxin B resistant protein A; PRE, paramagnetic relaxation enhancement; PmrD, polymixin B resistant protein D; $PmrA_N$, the N-terminal receiver domain of PmrA; HDX, hydrogen/deuterium exchange; r.m.s.d, root mean square deviation; MTSL, (1-oxyl-2,2,5,5-tetramethyl-3-pyrroline-3-methyl)-methanethiosulfonate).

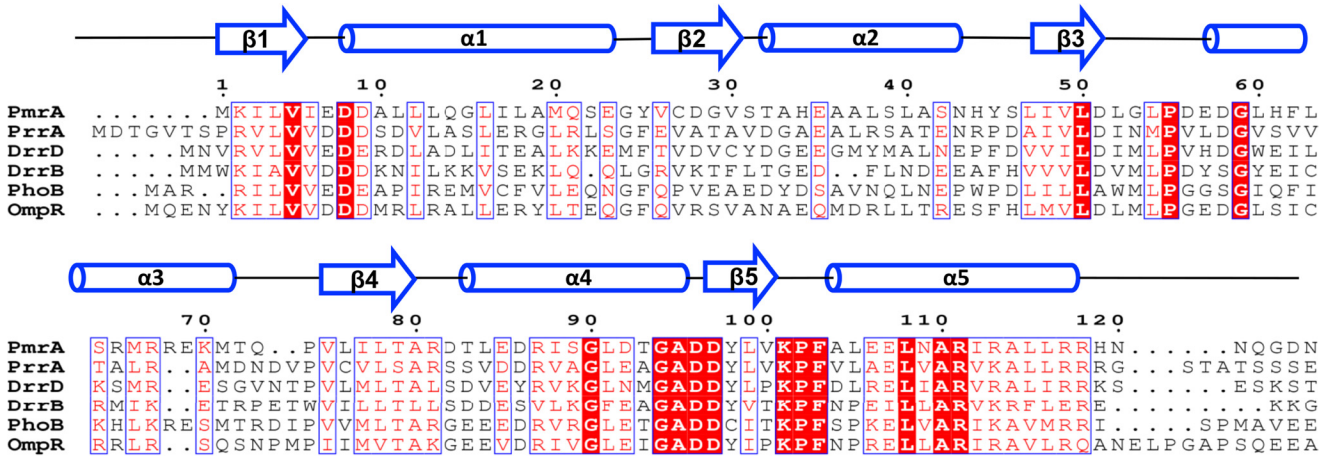

FIGURE 1. **Primary sequence alignment of N-terminal receiver domains of PmrA and five other response regulators.** The secondary structural elements of $PmrA_N$ are at the *top* of the figure. Identical residues are shown in *white* with a *red* background, and similar residues are shown in *red*. The alignment was generated by use of CLUSTAL-W (60) and ESPript (61).

response regulator is protected by the connector protein in the interconnecting signal transduction pathways such as PmrD and phospho-PmrA.

Previously, we determined the solution structure for *K. pneumoniae* PmrD and mapped its binding sites when it bound to $PmrA_N$ (18). In this study, we present the structure of the BeF_3^--activated N-terminal receiver domain of PmrA ($PmrA_N$) solved by x-ray crystallography. The backbone assignment of $PmrA_N$ involved transverse relaxation-optimized spectroscopy-type three-dimensional NMR experiments with ^2H,^{13}C,^{15}N-labeled $PmrA_N$. With the chemical shift perturbations of $PmrA_N$ when binding with PmrD and structures of PmrD and $PmrA_N$, we used HADDOCK (19) to generate a complex structure of the PmrD-$PmrA_N$ heterotetramer. Furthermore, using NMR hydrogen/deuterium exchange (HDX) exchange studies combined with a paramagnetic spin-labeling approach, we further confirmed the reliability of this complex model. We found that $PmrA_N$ interacts with PmrD via the residues near the active sites that are widely used by response regulators for intermolecular protein-protein interactions with histidine kinase. The results of this study can help reveal the molecular mechanisms of the interaction mode between connector proteins and phosphorylated response regulators in TCSs.

EXPERIMENTAL PROCEDURES

Cloning, Expression, and Purification of the Recombinant Proteins—The coding regions of *pmr* and $PmrA_N$ (N-terminal 123 residues) were PCR-amplified from the genomic DNA of *K. pneumoniae.* The amplified gene products were cloned as an NdeI/XhoI fragment into the pET29b vector (Novagene). The resulting plasmids (pET-PmrD and pET-$PmrA_N$) allowed for the in-frame fusion of each coding region containing an additional LEHHHHHH sequence at the C terminus to facilitate protein purification. The recombinant proteins were overexpressed in the host *E. coli* strain BL21(DE3) (Novagen) induced with 1 mM isopropyl 1-thio-β-D-galactopyranoside at 37 °C (for PmrD) or 30 °C ($PmrA_N$). After lysis with use of an M-110S microfluidizer (Microfluidics) and subsequent centrifugation, the overproduced proteins were purified from the soluble fraction by affinity chromatography on His-Bind resin (Novagene) and size-exclusion chromatography with a Superdex75 10/300 GL column. The eluted samples were dialyzed against 50 mM Tris (pH 8.0), 100 mM NaCl, and concentrated by use of Amicon (molecular weight of 5000; Millipore). For isotopically enriched samples, cells were grown in M9 minimal medium (20) containing 1 g/liter $^{15}NH_4Cl$ and 2 g/liter [^{13}C]glucose. PmrD and $PmrA_N$ mutants were generated according to QuikChange™ protocol (Stratagene). The authenticity of the recombinant proteins was verified by SDS-PAGE and mass spectrometry.

Crystallization of BeF_3^--activated $PmrA_N$—For crystallization trials, the BeF_3^--activated $PmrA_N$ was first concentrated to 5 mg/ml in buffer containing 20 mM sodium phosphate, pH 6.0, and 30 mM NaCl with use of a Centricon concentrator (Millipore). The BeF_3^--activated $PmrA_N$ was obtained by adding 5.3 mM $BeCl_2$ (Fluka), 35 mM NaF, and 7 mM $MgCl_2$. The hanging drop vapor diffusion method was then performed at 298 K by mixing 1 μl BeF_3^--activated $PmrA_N$ with an equal volume of crystal screening solutions. Hexagonal crystals appeared after 3 days under the condition of 100 mM imidazole and 1 M sodium acetate at pH 6.5. The crystals belong to space group *P*41 and contain one $PmrA_N$ dimer per asymmetric unit. Collection of the cryogenic multiwavelength anomalous dispersion data involved use of an Area Detector Systems Quantum-315 charge-coupled device detector with a synchrotron radiation x-ray source at beamline BL13B1 at the National Synchrotron Radiation Research Center in Taiwan. X-ray diffraction data integration and scaling involved use of the HKL2000 package (21). The extension of initial phases to 1.99 Å and the preliminary auto-model building involved use of RESOLVE (22). XtalView (23) was used to examine electron density maps and for manual model building. Further refinement involved use of CNS (24) and PHENIX (25). After completion, the R_{factor} of the final model for all reflections above 1σ between 25.38 and 1.70 Å resolution was refined to 16.5%, and an R_{free} value of 17.5% was obtained with 5.2% randomly distributed reflections (26). The structures were visualized and plotted with use of PyMOL (27).

NMR Backbone Resonance Assignments of Free and Bound Forms of BeF_3^--activated $PmrA_N$—NMR experiments with 0.3 mM ^2H,^{13}C,^{15}N-labeled $PmrA_N$ or in complex with PmrD (with

a molar ratio of 1:2) in a Shigemi NMR tube (Allison Park, PA) were performed at 310 K with the use of Bruker AVANCE 600 and 800 NMR spectrometers (Bruker, Karlsruhe, Germany) equipped with a triple (^{1}H, ^{13}C, and ^{15}N) resonance cryoprobe including a shielded z-gradient. All heteronuclear NMR experiments were performed as described (28). Sequence-specific assignment of the backbone atoms was achieved by independent connective analysis of transverse relaxation-optimized spectroscopy-type three-dimensional HNCA, HN(CO)CA, CBCA(CO)NH, HNCACB, HNCO, and HN(CA)CO experiments. The chemical shifts of individual spin systems (HN, N, Cα, Cβ, C′, and Hα) were collected manually, and the backbone resonances were assigned by visual inspection. Transverse relaxation-optimized spectroscopy-based NOESY and HNCO spectra were acquired on the triple-labeled PmrA$_N$ in complex with PmrD. From the resonance assignments for free PmrA$_N$, most of the resonances in the bound PmrA$_N$ could be easily identified because their cross-peaks were well superimposed. For the residues with significant shift perturbations, their backbones were assigned by comparing NOE connectivities and carbonyl carbon chemical shifts between the free and bound forms. All NMR spectra were processed and analyzed by use of Topspin (Bruker Biospin), NMRPipe (29), and NMRView (30) software packages.

HDX Experiments—HDX experiments were initiated by adding D_2O (99.9%) to lyophilized protein, which had been prepared at the required pH and buffer conditions. The concentration of ^{15}N,^{13}C,^{2}H-labeled PmrA$_N$ was ~100 μM, and the unlabeled PmrD was ~200 μM. The ^{15}N-^{1}H selective optimized flip-angle short-transient heteronuclear multiple quantum coherence procedure (31) was used to obtain the ^{15}N-^{1}H correlation spectra with 1024 (t_2) and 64 (t_1) complex points and 4 scans at 310 K.

Chemical Shift Perturbation Experiments—To map the binding sites on PmrA$_N$ with PmrD, we collected ^{1}H-^{15}N HSQC spectra for ^{2}H,^{15}N-labeled PmrA$_N$ with unlabeled PmrD at a molar ratio of 1:2. We investigated and ruled out the possibility that the shift changes of PmrD were due to constituents of BeF_3^-. All spectra processing were analyzed by use of XWIN-NMR (Bruker Biospin) and SPARKY (32). Normalized chemical shift changes were calculated as follows.

$$\Delta\delta = [\Delta H^2 + (0.17\Delta N)^2]^{1/2} \quad \text{(Eq. 1)}$$

The cut-off (0.135 ppm) was set as the S.D. for all chemical shift changes. All residues with values above the cut-off were considered affected by interaction with PmrD.

Complex Structure Determination using HADDOCK—The information-driven docking program HADDOCK (version 2.0) (19) was used to generate a PmrD-PmrA$_N$ complex model. The starting structures for docking were an x-ray crystal structure of PmrA$_N$ and the 10 lowest energy structures of PmrD, which were refined with the constraints measured from the chemical shift perturbations (18). From NMR titration data, different sets of ambiguous interaction restraints were used to generate the complex model. PmrD contained sets that included the active residues 4, 26, 48, 49, 50, 52, 67, 70, 71, 73, and 74 and passive residues 1, 24, 47, 64, and 66. The PmrA$_N$ model contained sets that included the active residues 8, 9, 53, 59, 99, 104, 105, 138, 139, 183, 189, 229, 234, and 236. The active residues were chosen on the basis of the chemical shift perturbation data and high solvent accessibility (>50%). The passive residues are the solvent-accessible surfaces neighboring active residues. During the rigid body energy minimization, 10,000 structures were calculated, and the 199 best solutions based on the intermolecular energy were used for the semi-flexible, simulated annealing, followed by explicit water refinement. The best 199 docked models were clustered by use of a cut-off r.m.s.d. of 3.5 Å. The clusters were ranked by the averaged HADDOCK score of their top 10 complex models (Table 1).

TABLE 1
Docking and structural statics for the best 199 and best 10 PmrD-PmrA$_N$ model structures

Docking statistics	Ensemble (199 structures)	Best 10 structures
Haddock score	−144.61 ± 19.86	−181.352 ± 4.61
E_{vdw} (kcal/mol)	−82.18 ± 8.16	−89.55 ± 8.22
E_{elec} (kcal/mol)	−550.71 ± 79.78	−694.77 ± 52.86
E_{inter}(kcal/mol)	−583.84 ± 80.92	−738.89 ± 51.84
E_{AIR} (kcal/mol)	48.24 ± 11.51	43.83 ± 3.37
BSA (Å^2)	3143.53 ± 151.53	3378.55 ± 157.648
r.m.s.d. from lowest energy structure (Å)	0.984	0.847 ± 0.33
No. of AIR violations > 0.3 Å	1.23 ± 0.47	1.1 ± 0.3
Deviations from idealized geometry		
r.m.s.d. for bond angles	0.5°	0.5°
r.m.s.d. for bond lengths (Å)	0.004	0.004
Ramachandran analysis, residues in		
Most favored regions (%)	82.2	82.9
Additionally allowed regions (%)	15.8	14.9
Generously allowed regions (%)	1.4	1.4
Disallowed regions (%)	0.6	0.8

Site-directed Spin Labeling and Paramagnetic Relaxation Enhancement (PRE) Experiments—PmrDC54 constructs containing a single cysteine residue were generated by use of site-directed mutagenesis to convert existing extra cysteine residues to serine. Mutations were confirmed by DNA sequencing over the entire open reading frame and were found to be properly folded and capable of binding BeF_3^--activated PmrA$_N$ as for wild-type PmrD. Purified mutants were modified with the thio-specific spin-label reagent MTSL ((1-oxyl-2,2,5,5-tetramethyl-3-pyrroline-3-methyl) methanethiosulfonate)) purchased from Affymetrix-Anatrace. The protein solution was added to a 20-fold molar excess of MTSL solution dissolved in acetone. The spin-labeling reactions were performed in the dark at room temperature overnight. Excess MTSL was removed by extensive dialysis, and the sample was concentrated to 150 μM. For NMR HSQC experiments, the complex was prepared with a molar ratio of 1:2 of ^{15}N,^{13}C,^{2}H triple-labeled PmrA$_N$: PmrDC54 with MTSL or ^{15}N,^{13}C,^{2}H triple-labeled PmrD: PmrA$_N$ D56C with MTSL. All experiments were repeated after the spin label was reduced with 5-fold excess concentrated ascorbic acid and DTT (2–5 μl from a concentrated stock; dilution < 1.25%) to NMR samples. Samples were placed at 25 °C for at least 1 h after the addition of reducing agent. The intensity ratios of paramagnetic *versus* diamagnetic spectra were obtained from the peak heights and further normalized before distance constraints were converted.

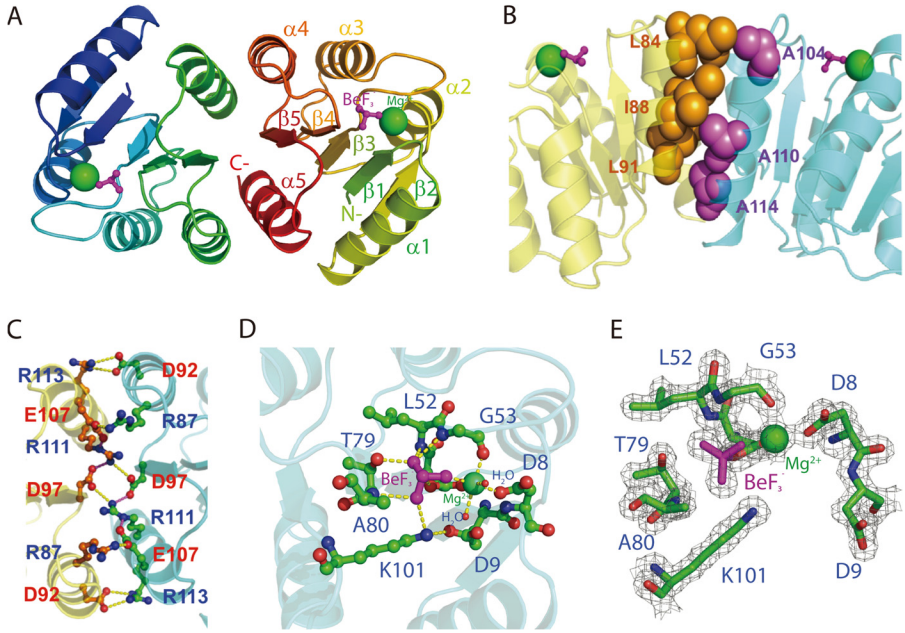

FIGURE 2. **X-ray crystal structure of $PmrA_N$.** *A*, ribbon structure of $PmrA_N$ shows the formation of a dimer with the interface at α4-β5-α5. The phosphate analog, BeF_3^-, is shown as a ball and stick figure in *magenta*, and Mg^{2+} is represented by a *green sphere*. *B*, hydrophobic interactions identified at the dimer interface. A hydrophobic patch (*spheres*) brings helices α4 (Leu-84, Leu-91, and Ile-88 colored in *orange*) and α5 (Ala-104, Ala-110, and Ala-114 colored in *purple*) together. *C*, the dimer interface is stabilized by an extensive network of salt bridges, Arg-87(α4)–Glu-107(α5), Asp-92(α4)–Arg-113(α5), and Asp-97(β5)–Arg-111(α5). *D*, an extended view of the active site. The Mg^{2+} is octahedrally coordinated to Asp-51, Gly-53, Asp-8, BeF_3^-, and two water molecules. The BeF_3^- moiety contacts with the side chain oxygen atom of Thr-79, the Nζ atom of Lys-101 and the backbone nitrogen atoms of Gly-53, Leu-52, and Ala-80. Carbon, oxygen, and nitrogen atoms are shown in *green*, *red*, and *blue*, respectively. *E*, active site electron density map ($F_o - F_c$) of the BeF_3^--activated $PmrA_N$ calculated at 2σ is shown in *gray* within 1.7 Å of the residues depicted in sticks.

RESULTS

Structure of $PmrA_N$ and Dimer Interface—Beryllium fluoride, a phosphoryl analog (33), was used to produce an activated form of $PmrA_N$ for structural studies. The structure of $PmrA_N$ was solved with experimental phases from molecular replacement data at 1.70 Å. The initial phases of $PmrA_N$ were solved with use of the molecular replacement software MOLREP from the CCP4 suite (34). The overall structure of $PmrA_N$ adopts a typically $(\beta\alpha)_5$ topology and follows the signature CheY-like α/β-fold architecture of receiver domains shared by all response regulators (35). Alternating β-strands and α-helices in the primary structure fold into a central five-stranded parallel β-sheet surrounded by two α-helices on one side and three on the other side (Fig. 2*A*). The asymmetric unit has only one molecule that forms a dimer with another crystallographic symmetry-related molecule using the face formed by helix α4, strand β5, and helix α5 (Fig. 2*A*). The presence of a large number of intra- and intermolecular interactions involving hydrophobic and polar residues was revealed by analysis of the interface. The α4 helix of one monomer packs against the α5 helix of the other monomer through a hydrophobic patch formed between Leu-84 (α4), Ile-88 (α4), and Leu-91 (α5) and the aliphatic portions of Ala-104 (α4), Ala-110 (α5), and Ala-114 (α5) side chains (Fig. 2*B*). The interface is further stabilized by a number of side chains involved in attributive salt bridges, especially toward the center region, which creates an extensive network that surrounds the hydrophobic packing between the α4 and α5 helices. Intermolecular salt bridges are formed between Arg-87(α4)–Glu-107(α5), Asp-92(α4)–Arg-113(α5), and Asp-97(β5)–Arg-111(α5) at the outer sides (Fig. 2*C*). The x-ray structures of other members of the activated form of receiver domains in the OmpR-PhoB subfamily were reported previously, including PhoB and PhoP from *E. coli* and DrrB and DrrD from *Thermotoga maritime* (36–38). In all cases, the receiver domains form a dimer with an interface at α4-β5-α5, which reveals a common dimerization mechanism on activation with members of the OmpR-PhoB subfamily.

Coordination of the Active Site in $PmrA_N$—PmrA is phosphorylated at Asp^{51}, the residue that corresponds to the conserved phosphorylation site shared by the receiver domains of response regulators (39). In the crystal structure, Mg^{2+} binds to F_1 of BeF_3^-, the side chain carboxyl oxygens of Asp-8 and Asp-51; the main chain carbonyl oxygen of Gly-53, a water molecule hydrogen-bonded to Asp-8 and another water molecule hydrogen-bonded to Asp-9, thus satisfying the octahedral coordination of Mg^{2+} (Fig. 2*D*). The BeF_3^- is non-covalently bound to Asp-51 centered within the active site. The conserved Lys-101 is involved in salt bridges with Asp-9 and F_3 of BeF_3^-. The conserved Thr-79 forming a hydrogen bond with the F_2 of BeF_3^-, involved in the activation mechanism in other response regulators, is in an inward orientation. The rotation of Thr-79 is accompanied by a rotation of the backbone N of the next residue, Ala-80, which forms a hydrogen bond with F_3 of BeF_3^-. Ser/Thr and Phe/Tyr located in the β4-α4 loop and β5 (Thr-79 and Tyr-98 in PmrA, Fig. 2*D*) are the signature aromatic "switch" residues involved in rearrangements associated with phosphorylation (3, 40). In the $PmrA_N$ structure, Thr-79 is oriented toward the active site to coordinate with BeF_3^-, whereas Tyr-98 adopts an inward position, forming a hydrogen bond with the main chain carbonyl oxygen of Arg-81 situated at the

TABLE 2
Data collection and refinement statistics

Data collection	
Space group	$P4_1$
Cell dimensions	$a = b$ 49.99 and c = 145.86 Å
Wavelength (Å)	0.97315
Resolution (Å)	1.7
Redundancy	12.2 (11.9)[a]
$I/\sigma(I)$	40.4 (6.7)[a]
Completeness (%)	97.2 (94.5)[a]
R_{merge} (%)	6.6 (41.7)
Refinement	
Resolution (Å)	25.38-1.70
No. of reflections	38,239
R_{work}/R_{free} (%)	16.5/17.5
No. of atoms	
Protein	2,232
Ligands	10
Water	424
B factors	
Protein	18.2
Ligands	14.6
Water	32.6
r.m.s.d.	
Bond lengths (Å)	0.006
Bond angles	1.09°
Ramachandran favored (%)	99
Ramachandran outliers (%)	0

[a] Numbers in parentheses refer to the highest resolution shell.

middle of the β4-α4 loop. Crystallographic data are summarized in Table 2, and electron density for the active site of the refined model is shown in Fig. 2*E*.

^{1}H, ^{13}C, and ^{15}N Assignments and Secondary Structure Comparisons between Solution and X-ray PmrA$_N$ Structures—We could not grow good crystals of PmrA$_N$ in complex with PmrD and therefore used NMR techniques to obtain detailed structural information and gain insight into the protein-protein interactions (41). Two-dimensional ^{15}N-^{1}H HSQC spectrum of PmrA$_N$ is well dispersed, which indicates a well folded structure. Following a standard sequential assignment procedure, all of the observed cross-peaks in the HSQC spectrum were completely assigned, which correspond to 97% of ^1H_N–^{15}N pairs (115 of 119). The four unassigned residues were His-44, Leu-105, Gln-122, and Gly-123. Their cross-peaks disappeared, presumably because of solvent exposure. For the other backbone atoms, 98% of $^1H\alpha$ resonances (116 of 119) and 98% of $^{13}C'$, $^{13}C\alpha$, and $^{13}C\beta$ resonances (351 of 360) were assigned. Hα of Arg-87 was shifted up-field at 3.54 ppm, which is likely due to the shielding effect by Tyr-98 as seen in the crystal structure. The chemical shift index (29) based on Hα, Cα, Cβ, and C′ chemical shifts showed that PmrA$_N$ contains four β-strands (residues 2–7, 47–51, 74–79, and 95–100) and five α-helices (residues 10–22, 34–41, 59–70, 84–92, and 104–120), which are similar to those in the crystal structure.

Interaction between PmrD and PmrA$_N$—Previously, we studied the binding stoichiometry of the PmrD-PmrA$_N$ complex in the presence of BeF_3^- (18). The binding ratio of 1:1 was determined by size-exclusion chromatography and ^{1}H transverse relaxation time measurements. The equilibrium dissociation constant of ~1 μM was measured by surface plasma resonance. To further identify the sites of interaction of PmrA$_N$ with PmrD, we performed chemical shift perturbation experiments, in which the chemical shift changes on the ^{15}N,^1H_N correlation plot of the BeF_3^--activated PmrA$_N$ were detected with the addition of 2-fold unlabeled PmrD (Fig. 3*A*). The addition of PmrD caused significant chemical shift changes, the intermediate exchange line broadening on several residues, and emerging cross-peaks for backbone ^{15}N and ^1H_N resonances. At a molar ratio of 1 to 0.9, two separate NMR signals, one for the free and the other for the bound form, were clearly seen for some residues such as Asp-9, Val-49, Asp-56, and Gln-73. Therefore, we suggested that the interaction belongs to the slow exchange regime on the NMR timescale. The backbone resonances of Lys-2 and Leu-12 were missing because of peak broadening beyond detection. Leu-105 was not observed in the free form but appeared in the presence of PmrD, which suggests lower solvent accessibility of the amide proton of Leu-105 in the complex. We found no significant intermolecular NOEs in the three-dimensional NOESY-HSQC spectra, which may be due to weak binding of the protein complex. A total of 14 residues of PmrA$_N$ showed significant perturbations with the addition of a 2-fold molar ratio of PmrD ($>$ 0.15 ppm) and were labeled on the chemical shift perturbation bar plot (Fig. 3*B*). Mapping these residues onto the structure showed that most of them are located near the phosphorylation site of PmrA$_N$, which comprises the β1-α1 loop, N-terminal α1, β3-α3 loop, N-terminal α3, C-terminal β4, β4-α4 loop, C-terminal β5, β5-α5 loop and N-terminal α5 (Fig. 3*C*).

HDX Study and Solvent Accessibility between the Free and Bound Forms of PmrA$_N$—HDX rates can provide information about the solvent accessibility for different backbone amide protons. Here we used HDX to map the binding interface in PmrD-PmrA$_N$. First, we used the free form of ^{15}N-labeled PmrA$_N$ for the HDX study and found that ~41 cross-peaks were water-inaccessible (Fig. 4*A*). Mapping these residues onto the PmrA$_N$ structure showed that they were mainly located on the central five-stranded parallel β-sheet or the interface mediated by the α4-β5-α5 face but not on the surface near the phosphorylation site. Next, we added unlabeled PmrD into ^{15}N-labeled PmrA$_N$ and repeated the same experiment under the same conditions and compared the results with the HDX data for free PmrA$_N$. Most of the water-inaccessible residues were similar to those in the free PmrA$_N$ (Fig. 4*B*), so these residues are not involved in binding with PmrD. However, three residues, Leu-11, Phe-103, and Arg-81, showed a lower water-accessible rate in the presence of PmrD (Fig. 4*B*), presumably because of the steric occlusion effect of PmrD. Interestingly, Leu-11, Arg-81, and Phe-103 are all close to the phosphorylation site and are consistent with the binding interface determined by chemical shift perturbation (Fig. 4*C*).

Modeling of the PmrD-PmrA$_N$ Complex—With formation of the PmrD-PmrA$_N$ complex, we observed significant broadening of NMR signals for both PmrD and PmrA$_N$, which may be due to the slower tumbling of the complex and/or a contribution from intermediate timescale chemical exchange broadening. These significantly broadened NMR resonances limited the acquisition of intermolecular NOEs critical for determining the structure of multiprotein complexes, although this effect aided in identifying interfacial residues. Because of a lack of intermolecular NOEs, we generated the complex model of a PmrD-PmrA$_N$ heterotetramer using the experimental data-driven docking method of HADDOCK (19). The generated complex

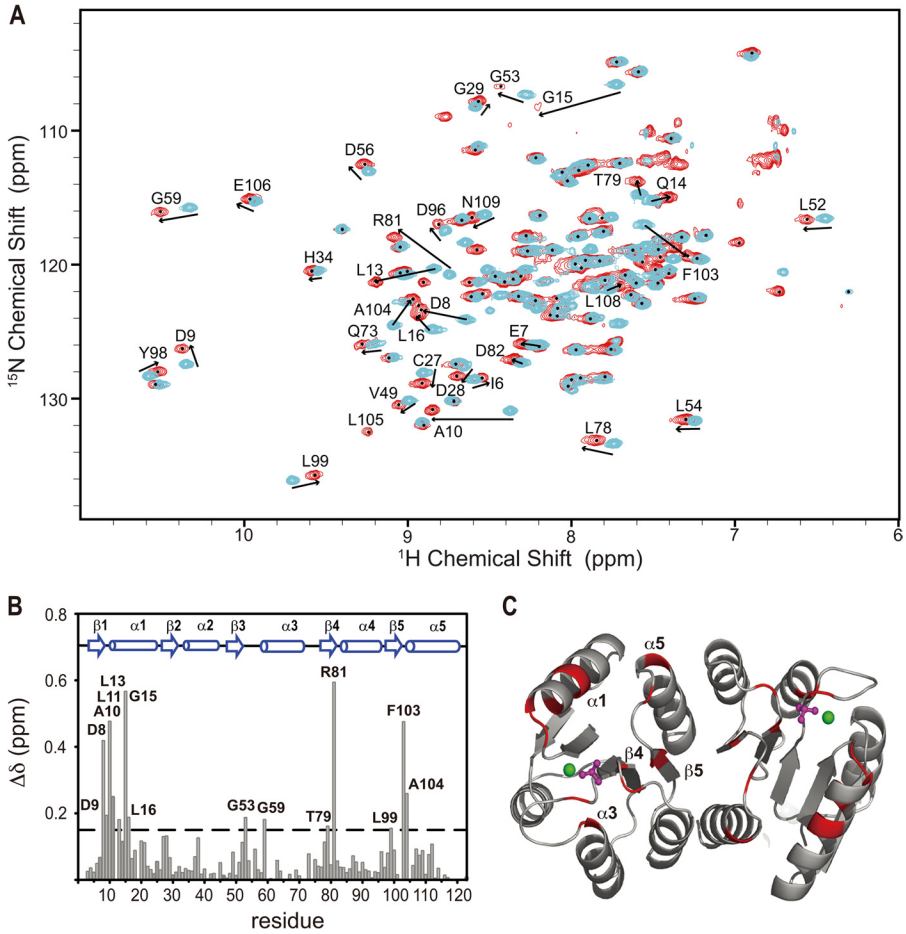

FIGURE 3. **The induced chemical shift perturbation of ^{2}H,^{15}N,^{13}C-labeled PmrA$_N$ with the presence of PmrD.** *A*, a section of overlaid ^{1}H,^{15}N TROSY-HSQC spectra of free PmrA$_N$ (*cyan*) binding to 2-fold molar ratio of unlabeled PmrD (*red*). The residues showing significant chemical shift perturbations are labeled with a one-letter code for amino acids with the residue number. *B*, graph representing the weighted average of the chemical shift differences between the free and PmrD-bound PmrA$_N$. The secondary structural elements of PmrA$_N$ are illustrated on *top*. *C*, ribbon structure of PmrA$_N$ with the residues showing weighted chemical shift perturbations > 0.135 ppm are in *red*.

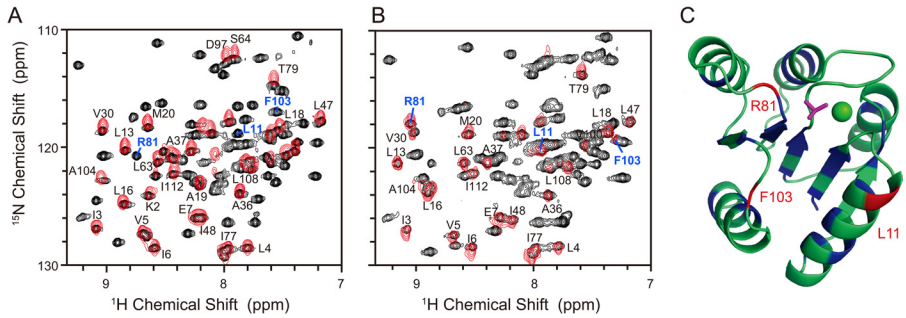

FIGURE 4. Shown is a hydrogen/deuterium exchange study on the free (*A*) and PmrD-bound (*B*) PmrA$_N$. The overlay of ^{1}H,^{15}N TROSY-HSQC spectra of protein samples incubated in 90% H_2O, 10% D_2O (*black*) or in 100% D_2O for 5 min (*red*). Three PmrA$_N$ residues, which are water-inaccessible in the bound form only, are labeled in *blue*. *C*, ribbon representation of PmrA$_N$ monomer. The residues that are water-inaccessible in the free PmrA$_N$ are colored in *blue*, and the three residues that were water-inaccessible only in the PmrD-bound PmrA$_N$ are colored and labeled in *red*.

model is dominated by intermolecular interactions between residues located on the active site pockets of PmrA$_N$ and the solvent-exposed face of the β-barrel of PmrD (Fig. 5*A*). Seven intermolecular hydrogen bonds were identified: Ser-23(HG)–Asp-9(OD1), Ser-23(HG)–Asp-9(OD2), Ala-49(O)–Leu-105(HN), Asn-67(OD1)–Thr-83(HN), His-70(HD1)–Gly-53(O), His-70(HE2)–Asp-9(OD1), and Arg-75(HH12)–Glu-85(OE2) (Fig. 5*B*). In addition, two intermolecular salt bridges were found between Lys-64–Glu-31 with 2-fold symmetry (Fig. 5*B*). Therefore, the hydrogen bonds and salt bridges for each partner interact with appropriately charged residues on the corresponding interface, providing a specificity of structural arrangement for the interaction between PmrD and PmrA$_N$.

PRE Effect of Site-directed Spin Labeling on PmrDC54 and PmrA$_N$ D56C—To double-confirm the orientations of the PmrD-PmrA$_N$ complex model, we used site-directed spin labeling with a nitroxide spin-label compound, MTSL, covalently attached to a Cys residue (42) for PRE experiments, which

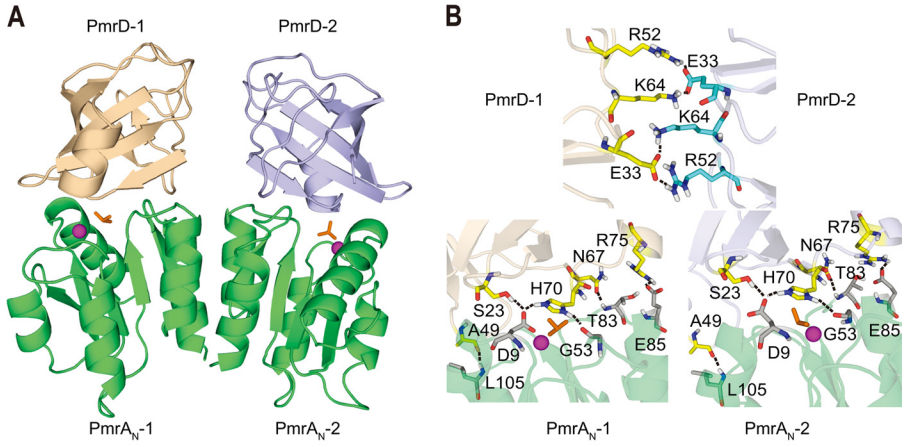

C

PmrD-1	PmrD-2	Salt bridge (out of 10)
33 Glu (OE1)	64 Lys (HZ1)	6
33 Glu (OE2)	52 Arg (HH21)	6
52 Arg (HH21)	33 Glu (OE2)	7
64 Lys (Hz1)	33 Glu (OE1)	8
64 Lys (Hz1)	33 Glu (OE2)	5

PmrD-1	PmrA$_N$-1	Hbond (out of 10)
23 Ser (HG)	9 Asp (OD1)	7
23 Ser (HG)	9 Asp (OD2)	5
49 Ala (O)	105 Leu (HN)	8
67 Asn (OD1)	83 Thr (HN)	7
70 His (HD1)	53 Gly (O)	10
70 His (HE2)	9 Asp (OD1)	8
75 Arg (HH12)	85 Glu (OE2)	5

PmrD-2	PmrA$_N$-2	Hbond (out of 10)
23 Ser (HG)	9 Asp (OD1)	8
49 Ala (O)	105 Leu (HN)	8
67 Asn (OD1)	83 Thr (HN)	7
70 His (HD1)	9 Asp (OD1)	7
70 His (HD1)	53 Gly (O)	6
75 Arg (HH12)	85 Glu (OE2)	7
74 Glu (OE1)	81 Arg (HH12)	6

FIGURE 5. *A*, HADDOCK-derived structural model of PmrD-PmrA$_N$ complex, with PmrD shown in *beige* and *light blue*, and the PmrA$_N$ dimer is shown in *lime green*. *B*, intermolecular interactions between the two PmrDs (*top*) and between PmrD and PmrA$_N$ (*bottom*) in the complex structure. *C*, summary of the intermolecular interactions between the two PmrDs (*top*) and between PmrD and PmrA$_N$ (*bottom*).

can be used as an independent biophysical method to obtain intermolecular long distance (<30 Å) information. PmrD contains three Cys residues (Cys-17, Cys-35, and Cys-54), and PmrA$_N$ contains only one Cys residue (Cys-27). To determine which Cys residues could be labeled under the conditions described under "Experimental Procedures," we initially covalently linked the stable mutant ^{15}N-labeled PmrD C35S and wild-type ^{15}N-labeled PmrA$_N$ using MTSL. The backbone HN of Cys-54 in PmrD C35S was significantly shifted as compared with PmrD, so Cys-54 was able to bind with MTSL. However, Cys-27 of PmrA$_N$ did not show any shift perturbation on adding MTSL, so Cys-27 is unlikely to bind to MTSL. We therefore produced two mutants, C17S/C35S on PmrD (PmrDC54) and D56C on PmrA$_N$ (PmrA$_N$ D56C), for PRE experiments. Spin labeling did not change the protein-protein interaction because the ^{1}H-^{15}N HSQC spectrum of PmrA$_N$ in complex with MTSL-labeled PmrDC54 with a reduced proxyl group was similar to that of PmrA$_N$ in complex with unlabeled PmrD (Fig. 6*A*) and vice versa. The unpaired electron of MTSL caused line-broadening effects on nearby residues in a distance-dependent manner. Line-broadening effects on the ^{15}N-labeled PmrA$_N$ were observed in the complexes with MTSL-labeled PmrDC54 (Fig. 6*A*). The superimposed spectra of the reduced (*black*) and oxidized (*red*) states showed significant R_2 relaxation enhancement effects. With the spin label on Cys-54 of PmrD, the signals on several residues of PmrA$_N$, such as Asp-82, Leu-84, Val-100, Phe-103, and Leu-105, were significantly reduced in the oxidized state (Fig. 6, *A* and *B*). Residues Asp-82, Leu-84, Val-100, and Phe-103 were all close to the active site of PmrA$_N$, as seen in the crystal structure. With MTSL attached to D56C of PmrA$_N$, three peaks corresponding to PmrD residues Gly-24–Ala-25 and the side chain amide peak of Trp-3 were severely attenuated (data not shown). These data suggest that the interaction brings the binding surface of PmrD (the open β-barrel area) (18) and the active site of PmrA$_N$ close to each other. In conclusion, the observed intermolecular PRE data are generally consistent with the HADDOCK-derived complex structure (Fig. 6*C*) and hence can provide an independent biophysical method to confirm the long range distance information between corresponding regions of the complex model.

DISCUSSION

Several crystal structures of receiver domains of response regulators have been solved (43–46), but little structural information is available regarding how they interact with each other in multiprotein complexes. As well, knowledge of the structure of the receiver domain in complex with the connector protein is limited. Several groups have reported that the active site from the receiver domain of the response regulator is widely used for intermolecular protein-protein interactions with histidine kinase. Here, we present the crystal structure of PmrA$_N$, in which a hydrogen bond couples with the carbonyl oxygen atom of Arg-81 situated on the β4-α4 loop and side chain of the aromatic residue Tyr-98, which is similar to the "T-loop-Y"

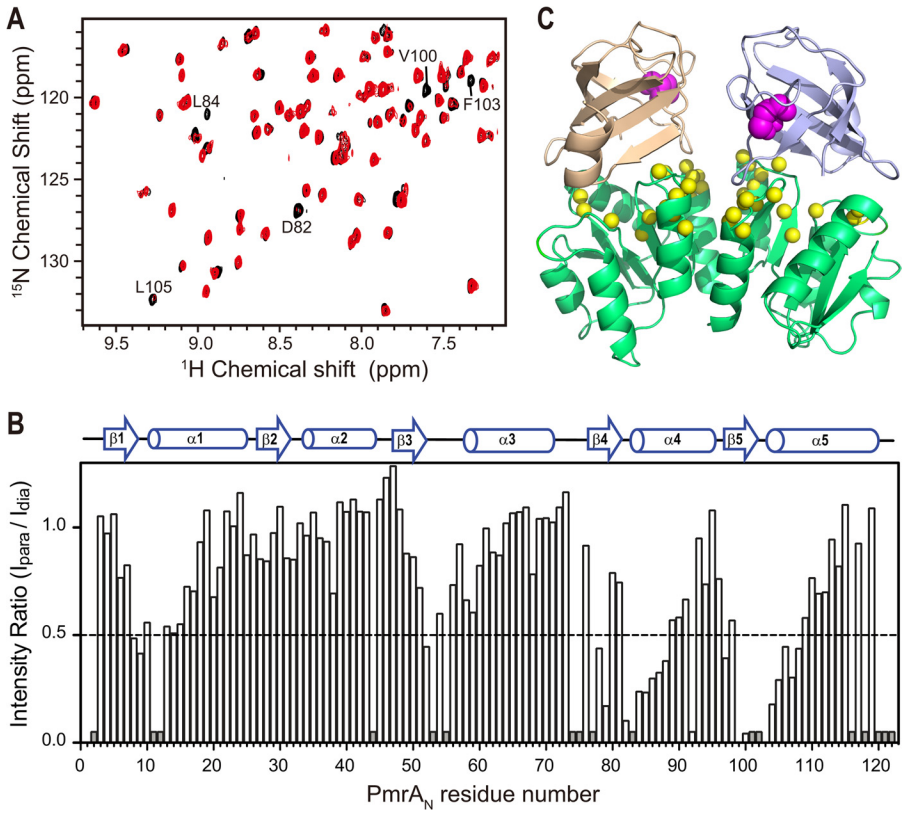

FIGURE 6. **PRE study on PmrD-PmrA$_N$ complex.** *A*, an expanded region of superimposed ^{1}H-^{15}N HSQC spectra of ^{15}N-labeled PmrA$_N$ in complex with PmrDC54 with (paramagnetic state, in *red*) or without (diamagnetic state, in *black*) MTSL spin labeling. The residues that disappeared in the paramagnetic state are labeled. *B*, a bar plot of intensity ratio of paramagnetic and diamagnetic cross-peaks (I_{para}/I_{dia}) *versus* residue number of PmrA$_N$. Unassigned and overlapped residues are shown as *short gray bars*. *C*, structural model of PmrD-PmrA$_N$ complex obtained by HADDOCK docking. The MTSL spin label sites, Cys-54 of two PmrDs, are shown as *magenta spheres*, and the PmrA$_N$ residues with $I_{para}/I_{dia} < 0.5$ are shown as *yellow spheres*.

model observed for the activation mechanism of a response regulator (47). In the model, the conformation of the β4-α4 loop was gated by phosphorylation and the position of the active site residue Thr-79, thus resulting in an inward orientation of the aromatic switch residue (47). Next, we demonstrated that PmrA$_N$ uses a similar surface to interact with the TCS connector protein PmrD (Fig. 7*A*). Therefore, PmrD is likely a competitive inhibitor of histidine kinase because it binds with the response regulator at a similar interface surrounding the phosphorylation site (48). In the PmrD-PmrA$_N$ complex model, the phosphoacceptor Asp-51 faces the open mouth area of the β-barrel of the PmrD structure, which reflects the protection mode of the connector protein on the phosphorylated response regulator. The orientation of PmrA$_N$ relative to PmrD can be attributed to three specific interactions. The first interaction is between the α1 and the β5-α5 loop region of PmrA$_N$ and loop 4 and N-terminal β1 in PmrD. The second interaction is between the β1-α1 loop of PmrA$_N$ and loop 2 of PmrD. The third interaction is between the β4-α4 loop and β3-α3 loop containing the Asp-51 phosphorylation site of PmrA$_N$ and C-terminal β6, loop 6, N-terminal β1, and β3 of PmrD. Interactions 2 and 3 create an environment that hides the phosphoryl analog of BeF_3^- between PmrD and PmrA$_N$. The binding interface of PmrA$_N$ is also similar to that observed in the crystal structure of the DHp domain in the ThkA-TrrA complex and Spo0F in the Spo0B-Spo0F complex from *Bacillus subtilis*, in which TrrA and Spo0F are the response regulators. In the PmrD-PmrA$_N$ complex, the phosphoacceptor Asp-51 in PmrA faces the His-70 of PmrD, similar to the phosphodonor His in the HK DHp domain (His-547 in ThkA) (48, 49). Hydrogen bonds and electrostatic interactions are important for stability and specificity of protein-protein interactions (50, 51). Consistently, we identified seven intermolecular hydrogen bonds and five salt bridges in our HADDOCK complex model (Fig. 5*C*), which emphasizes the role these interactions play in the recognition and specificity of PmrD connector proteins.

With response regulators, the phosphatase reaction is generally considered to proceed essentially as a reversal of the phospho-His phosphotransfer reaction, with water or hydroxide taking the place of the histidine imidazole side chain (52). Some of the histidine kinases have phosphatase activities toward their respective phosphorylated response regulators. The dephosphorylated kinases could promote a transition state with water in place of the phosphorylated histidine side chain, leading to hydrolysis instead of phosphorylation (53). For example, the structural basis of the response regulator Spo0F dephosphorylation by RapH phosphatases was revealed by the RapH-Spo0F crystal structure (Fig. 7*B*). In the structure, the side chain of RapH Gln-47 inserts into the Spo0F active site. RapH Gln-47 may orient water for direct in-line hydrophilic attack on the Spo0F phosphoaspartate 54 phosphorous atom and thus cause hydrolysis of the phosphoryl group (54). In these cases, the interactions are primarily responsible for the specific histidine

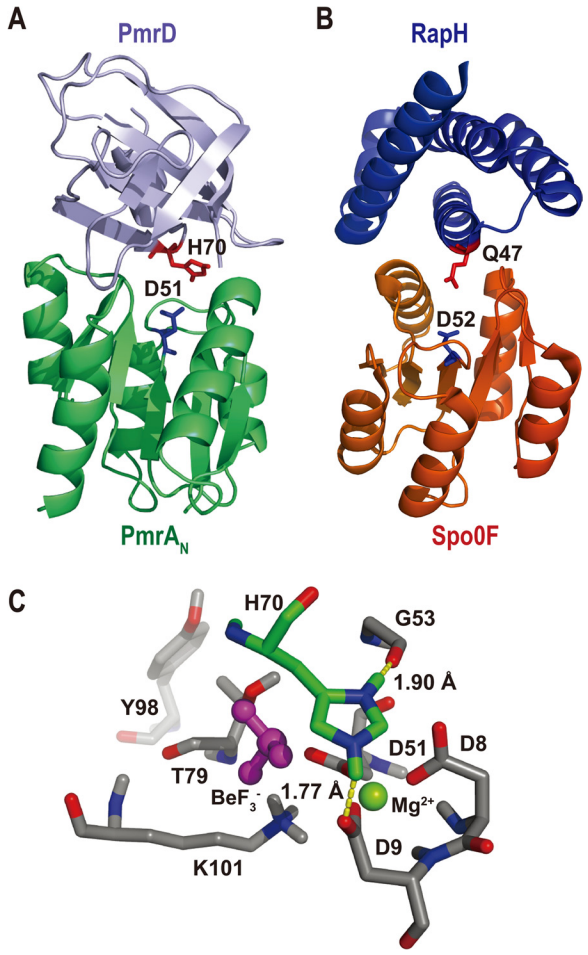

FIGURE 7. **A proposed physical blockage mechanism of PmrA dephosphorylation inhibited by PmrD.** *A*, the monomeric form of the PmrD-PmrA$_N$ complex is shown. His-70 of PmrD and Asp-51 from PmrA$_N$ are in *red* and *blue*, respectively. *B*, the crystal structure of the response regulator Spo0F in complex with the RapH phosphatase. The phosphorylation site Asp-52 is shown in *blue*, and the residue Gln-47 in RapH, which is responsible for dephosphorylating Spo0F, is in *red*. *C*, a stick diagram shows the intermolecular interactions near the active site residue Asp-51 of PmrA$_N$. The nitrogen and oxygen atoms are in *blue* and *red*, respectively. The carbon atoms of His-70 from PmrD are in *green* and are colored *gray* for others. The Hδ1 and Hϵ2 of His-70 in PmrD form H-bonds (*yellow dashed lines*) with the carbonyl groups of two active site residues (Asp-9 and Gly-53) of PmrA$_N$. The interactions demonstrate how PmrD can protect the phosphate group analog BeF_3^- (*magenta*) and the divalent cation Mg^{2+} (*green sphere*) on PmrA$_N$ and prevent it from dephosphorylation.

kinase-response regulator or connector-response regulator binding.

The receiver domain of PmrA could form a cooperative, intermolecular dimer of a response regulatory component that interacts to convert an inherently weak set of protein-protein interactions into a stronger binding force that permits the formation of a functional viable complex. Activation of a response regulator by a "pre-existing population shift" may be a general mechanism for two-component signaling (55). Selective binding to a low populated conformation hidden with traditional structural methods may be a general model for ligand binding (56). Therefore, PmrD may selectively bind to the phosphorylated higher energy active conformation of PmrA$_N$ and prevents its dephosphorylation by phosphatase such as PmrB.

In our previous study, we proposed a model of the PmrD-PmrA$_N$ protein complex and examined how PmrD regulates phospho-PmrA. Here, we propose that PmrD is a phosphatase inhibitor that specifically binds the phosphorylated active site and acts as a molecular barricade that inhibits interaction between the phosphatase and phosphorylatable Asp residue of PmrA and thus prevents intermolecular dephosphorylation. PmrD might inhibit dephosphorylation by sterically hindering the transfer of phosphate from Asp-51 of PmrA to phosphatase PmrB. The large size of PmrD and its predicted binding interface with PmrA are consistent with the model that inhibition occurs by a steric hindrance. The model shows three H-bonds between PmrD and residues near phosphorylation sites of PmrA$_N$. For example, the HD1 of His-70 in PmrD formed H-bonds with the carbonyl group of Gly-53 in PmrA$_N$. In addition, the Hϵ2 of His-70 in PmrD formed an H-bond with OD1 of Asp-9 in PmrA$_N$ (Fig. 7*C*). A divalent cation close to the active site is required to add or remove phosphoryl groups in the receiver domain of a response regulator (57). Therefore, the steric hindrance effect provided by PmrD could prevent the dephosphorylation of PmrA mediated by the cation. As well, nucleophilic attack by a water molecule is the likely mechanism of autodephosphorylation in response regulators (58, 59). The side chain of His-70 in PmrD likely maintains the phosphoryl group stability by sterically inhibiting access of the water molecule, which executes a nucleophilic attack on the phosphorus and causes hydrolysis of the phosphoryl group. These interactions may explain how PmrD stabilizes the activated PmrA$_N$ protein and thus prevents dephosphorylation of phosphate on Asp-51 from a phosphatase such as PmrB. PmrD may inhibit dephosphorylation of the response regulator by acting as a simple physical blockade to sterically block access to the phosphoacceptor Asp residue on the receiver domain of the response regulator, thus precluding close contact of phosphatase with the phosphorylation site on PmrA$_N$.

Acknowledgments—The NMR spectra were obtained at the High Field Nuclear Magnetic Resonance Center supported by the National Research Program for Genomic Medicine. We thank Laura Smales for copyediting the manuscript. We are grateful for access to synchrotron radiation beamlines BL13B1 at the National Synchrotron Radiation Research Center in Taiwan.

REFERENCES

1. Perraud, A. L., Weiss, V., and Gross, R. (1999) Signalling pathways in two-component phosphorelay systems. *Trends Microbiol.* **7,** 115–120
2. Stock, A. M., Robinson, V. L., and Goudreau, P. N. (2000) Two-component signal transduction. *Annu. Rev. Biochem.* **69,** 183–215
3. West, A. H., and Stock, A. M. (2001) Histidine kinases and response regulator proteins in two-component signaling systems. *Trends Biochem. Sci.* **26,** 369–376
4. Wurgler-Murphy, S. M., and Saito, H. (1997) Two-component signal transducers and MAPK cascades. *Trends Biochem. Sci.* **22,** 172–176
5. Hoch, J. and Silhavy, T. (eds) (1995) *Two-Component Signal Transduction*, pp. 129–144, ASM Press, Washington, D.C.
6. Roland, K. L., Martin, L. E., Esther, C. R., and Spitznagel, J. K. (1993) Spontaneous pmrA mutants of *Salmonella typhimurium LT2* define a new two-component regulatory system with a possible role in virulence. *J. Bacteriol.* **175,** 4154–4164
7. Kox, L. F., Wösten, M. M., and Groisman, E. A. (2000) A small protein that mediates the activation of a two-component system by another two-component system. *EMBO J.* **19,** 1861–1872

8. Wösten, M. M., Kox, L. F., Chamnongpol, S., Soncini, F. C., and Groisman, E. A. (2000) A signal transduction system that responds to extracellular iron. *Cell* **103,** 113–125
9. Perez, J. C., and Groisman, E. A. (2007) Acid pH activation of the PmrA/PmrB two-component regulatory system of *Salmonella enterica*. *Mol. Microbiol.* **63,** 283–293
10. Helander, I. M., Kato, Y., Kilpeläinen, I., Kostiainen, R., Lindner, B., Nummila, K., Sugiyama, T., and Yokochi, T. (1996) Characterization of lipopolysaccharides of polymyxin-resistant and polymyxin-sensitive *Klebsiella pneumoniae O3*. *Eur. J. Biochem.* **237,** 272–278
11. Zhou, Z., Ribeiro, A. A., Lin, S., Cotter, R. J., Miller, S. I., and Raetz, C. R. (2001) Lipid A modifications in polymyxin-resistant *Salmonella typhimurium*: PMRA-dependent 4-amino-4-deoxy-L-arabinose, and phosphoethanolamine incorporation. *J. Biol. Chem.* **276,** 43111–43121
12. Asensio, A., Oliver, A., González-Diego, P., Baquero, F., Pérez-Díaz, J. C., Ros, P., Cobo, J., Palacios, M., Lasheras, D., and Cantón, R. (2000) Outbreak of a multiresistant *Klebsiella pneumoniae* strain in an intensive care unit: antibiotic use as risk factor for colonization and infection. *Clin. Infect. Dis.* **30,** 55–60
13. Kato, A., and Groisman, E. A. (2004) Connecting two-component regulatory systems by a protein that protects a response regulator from dephosphorylation by its cognate sensor. *Genes Dev.* **18,** 2302–2313
14. Mitrophanov, A. Y., and Groisman, E. A. (2008) Signal integration in bacterial two-component regulatory systems. *Genes Dev.* **22,** 2601–2611
15. Itou, J., Eguchi, Y., and Utsumi, R. (2009) Molecular mechanism of transcriptional cascade initiated by the EvgS/EvgA system in *Escherichia coli K-12*. *Biosci. Biotechnol. Biochem.* **73,** 870–878
16. Bougdour, A., Cunning, C., Baptiste, P. J., Elliott, T., and Gottesman, S. (2008) Multiple pathways for regulation of sigmaS (RpoS) stability in *Escherichia coli* via the action of multiple anti-adaptors. *Mol. Microbiol.* **68,** 298–313
17. Gerken, H., Charlson, E. S., Cicirelli, E. M., Kenney, L. J., and Misra, R. (2009) MzrA: a novel modulator of the EnvZ/OmpR two-component regulon. *Mol. Microbiol.* **72,** 1408–1422
18. Luo, S. C., Lou, Y. C., Cheng, H. Y., Pan, Y. R., Peng, H. L., and Chen, C. (2010) Solution structure and phospho-PmrA recognition mode of PmrD from *Klebsiella pneumoniae*. *J. Struct. Biol.* **172,** 319–330
19. Dominguez, C., Boelens, R., and Bonvin, A. M. (2003) HADDOCK: a protein-protein docking approach based on biochemical or biophysical information. *J. Am. Chem. Soc.* **125,** 1731–1737
20. Sambrook, J., Fritsch, E. F., and Maniatis, T. (1989) *Molecular Cloning: A Laboratory Manual*, 2nd Ed., Vol. 3, p. A3, Cold Spring Harbor Laboratory, Cold Spring Harbor, NY
21. Otwinowski, Z., and Minor, W. (1997) Processing of x-ray diffraction data collected in oscillation mode in *Methods in Enzymology* (Charles W. Carter, Jr., ed.), pp. 307–326, Academic Press, New York
22. Terwilliger, T. (2000) Maximum-likelihood density modification. *Acta Crystallogr. D Biol. Crystallogr.* **56,** 965–972
23. McRee, D. E. (1999) XtalView Xfit - A versatile program for manipulating atomic coordinates and electron density. *J. Struct. Biol.* **125,** 156–165
24. Brünger, A. T., Adams, P. D., Clore, G. M., DeLano, W. L., Gros, P., Grosse-Kunstleve, R. W., Jiang, J. S., Kuszewski, J., Nilges, M., Pannu, N. S., Read, R. J., Rice, L. M., Simonson, T., and Warren, G. L. (1998) Crystallography & NMR system: A new software suite for macromolecular structure determination. *Acta Crystallogr. D Biol. Crystallogr.* **54,** 905–921
25. Adams, P. D., Afonine, P. V., Bunkóczi, G., Chen, V. B., Davis, I. W., Echols, N., Headd, J. J., Hung, L. W., Kapral, G. J., Grosse-Kunstleve, R. W., McCoy, A. J., Moriarty, N. W., Oeffner, R., Read, R. J., Richardson, D. C., Richardson, J. S., Terwilliger, T. C., and Zwart, P. H. (2010) PHENIX: a comprehensive Python-based system for macromolecular structure solution. *Acta Crystallogr. D Biol. Crystallogr.* **66,** 213–221
26. Afonine, P. V., Grosse-Kunstleve, R. W., Echols, N., Headd, J. J., Moriarty, N. W., Mustyakimov, M., Terwilliger, T. C., Urzhumtsev, A., Zwart, P. H., and Adams, P. D. (2012) Towards automated crystallographic structure refinement with phenix.refine. *Acta Crystallogr. D Biol. Crystallogr.* **68,** 352–367
27. DeLano, W. L. (2010) *The PyMOL Molecular Graphics System*, version 1.3r1, Schrödinger, LLC, New York
28. Kay, L. E. (1995) Pulsed field gradient multi-dimensional NMR methods for the study of protein structure and dynamics in solution. *Prog. Biophys. Mol. Biol.* **63,** 277–299
29. Delaglio, F., Grzesiek, S., Vuister, G. W., Zhu, G., Pfeifer, J., and Bax, A. (1995) NMRPipe: a multidimensional spectral processing system based on UNIX pipes. *J. Biomol. NMR* **6,** 277–293
30. Johnson, B. A., and Blevins, R. A. (1994) NMR View: A computer program for the visualization and analysis of NMR data. *J. Biomol. NMR* **4,** 603–614
31. Schanda, P., Kupce, E., and Brutscher, B. (2005) SOFAST-HMQC experiments for recording two-dimensional heteronuclear correlation spectra of proteins within a few seconds. *J. Biomol. NMR* **33,** 199–211
32. Goddard, T. D. and Kneller, D. G. (2008) SPARKY 3, University of California, San Francisco
33. Yan, D., Cho, H. S., Hastings, C. A., Igo, M. M., Lee, S. Y., Pelton, J. G., Stewart, V., Wemmer, D. E., and Kustu, S. (1999) Beryllofluoride mimics phosphorylation of NtrC and other bacterial response regulators. *Proc. Natl. Acad. Sci. U.S.A.* **96,** 14789–14794
34. Collaborative Computational Project, Number 4 (1994) The CCP4 suite: programs for protein crystallography. *Acta Crystallogr. D Biol. Crystallogr.* **50,** 760–763
35. Volz, K. (1993) Structural conservation in the CheY superfamily. *Biochemistry* **32,** 11741–11753
36. Bachhawat, P., and Stock, A. M. (2007) Crystal structures of the receiver domain of the response regulator PhoP from *Escherichia coli* in the absence and presence of the phosphoryl analog beryllofluoride. *J. Bacteriol.* **189,** 5987–5995
37. Barbieri, C. M., Mack, T. R., Robinson, V. L., Miller, M. T., and Stock, A. M. (2010) Regulation of response regulator autophosphorylation through interdomain contacts. *J. Biol. Chem.* **285,** 32325–32335
38. Bachhawat, P., Swapna, G. V., Montelione, G. T., and Stock, A. M. (2005) Mechanism of activation for transcription factor PhoB suggested by different modes of dimerization in the inactive and active states. *Structure* **13,** 1353–1363
39. Cho, H. S., Pelton, J. G., Yan, D., Kustu, S., and Wemmer, D. E. (2001) Phosphoaspartates in bacterial signal transduction. *Curr. Opin. Struct. Biol.* **11,** 679–684
40. Robinson, V. L., Buckler, D. R., and Stock, A. M. (2000) A tale of two components: a novel kinase and a regulatory switch. *Nat. Struct. Biol.* **7,** 626–633
41. O'Connell, M. R., Gamsjaeger, R., and Mackay, J. P. (2009) The structural analysis of protein-protein interactions by NMR spectroscopy. *Proteomics* **9,** 5224–5232
42. Battiste, J. L., and Wagner, G. (2000) Utilization of site-directed spin labeling and high-resolution heteronuclear nuclear magnetic resonance for global fold determination of large proteins with limited nuclear overhauser effect data. *Biochemistry* **39,** 5355–5365
43. Buckler, D. R., Zhou, Y., and Stock, A. M. (2002) Evidence of intradomain and interdomain flexibility in an OmpR/PhoB homolog from *Thermotoga maritima*. *Structure* **10,** 153–164
44. Toro-Roman, A., Mack, T. R., and Stock, A. M. (2005) Structural analysis and solution studies of the activated regulatory domain of the response regulator ArcA: a symmetric dimer mediated by the α4-β5-α5 face. *J. Mol. Biol.* **349,** 11–26
45. Bent, C. J., Isaacs, N. W., Mitchell, T. J., and Riboldi-Tunnicliffe, A. (2004) Crystal structure of the response regulator 02 receiver domain, the essential YycF two-component system of *Streptococcus pneumoniae* in both complexed and native states. *J. Bacteriol.* **186,** 2872–2879
46. Birck, C., Chen, Y., Hulett, F. M., and Samama, J. P. (2003) The crystal structure of the phosphorylation domain in PhoP reveals a functional tandem association mediated by an asymmetric interface. *J. Bacteriol.* **185,** 254–261
47. Dyer, C. M., and Dahlquist, F. W. (2006) Switched or not?: the structure of unphosphorylated CheY bound to the N terminus of FliM. *J. Bacteriol.* **188,** 7354–7363
48. Yamada, S., Sugimoto, H., Kobayashi, M., Ohno, A., Nakamura, H., and Shiro, Y. (2009) Structure of PAS-linked histidine kinase and the response regulator complex. *Structure* **17,** 1333–1344
49. Varughese, K. I., Tsigelny, I., and Zhao, H. (2006) The crystal structure of

beryllofluoride Spo0F in complex with the phosphotransferase Spo0B represents a phosphotransfer pretransition state. *J. Bacteriol.* **188,** 4970–4977
50. Janin, J., and Chothia, C. (1976) Stability and specificity of protein-protein interactions: the case of the trypsin-trypsin inhibitor complexes. *J. Mol. Biol.* **100,** 197–211
51. Chothia, C., Wodak, S., and Janin, J. (1976) Role of subunit interfaces in the allosteric mechanism of hemoglobin. *Proc. Natl. Acad. Sci. U.S.A.* **73,** 3793–3797
52. Lukat, G. S., Lee, B. H., Mottonen, J. M., Stock, A. M., and Stock, J. B. (1991) Roles of the highly conserved aspartate and lysine residues in the response regulator of bacterial chemotaxis. *J. Biol. Chem.* **266,** 8348–8354
53. Stock, J. B., Ninfa, A. J., and Stock, A. M. (1989) Protein phosphorylation and regulation of adaptive responses in bacteria. *Microbiol. Rev.* **53,** 450–490
54. Parashar, V., Mirouze, N., Dubnau, D. A., and Neiditch, M. B. (2011) Structural basis of response regulator dephosphorylation by Rap phosphatases. *PLoS Biol.* **9,** e1000589
55. Stock, A. M., and Guhaniyogi, J. (2006) A new perspective on response regulator activation. *J. Bacteriol.* **188,** 7328–7330
56. Li, P., Martins, I. R., Amarasinghe, G. K., and Rosen, M. K. (2008) Internal dynamics control activation and activity of the autoinhibited Vav DH domain. *Nat. Struct. Mol. Biol.* **15,** 613–618
57. Bourret, R. B. (2010) Receiver domain structure and function in response regulator proteins. *Curr. Opin. Microbiol.* **13,** 142–149
58. Stock, A. M., Martinez-Hackert, E., Rasmussen, B. F., West, A. H., Stock, J. B., Ringe, D., and Petsko, G. A. (1993) Structure of the Mg^{2+}-bound form of CheY and mechanism of phosphoryl transfer in bacterial chemotaxis. *Biochemistry* **32,** 13375–13380
59. Wolanin, P. M., Webre, D. J., and Stock, J. B. (2003) Mechanism of phosphatase activity in the chemotaxis response regulator CheY. *Biochemistry* **42,** 14075–14082
60. Thompson, J. D., Higgins, D. G., and Gibson, T. J. (1994) Improved sensitivity of profile searches through the use of sequence weights and gap excision. *Comput. Appl. Biosci.* **10,** 19–29
61. Gouet, P., Courcelle, E., Stuart, D. I., and Métoz, F. (1999) ESPript: analysis of multiple sequence alignments in PostScript. *Bioinformatics* **15,** 305–308